REPORT NO. FRA-RT-73-15

SIMULATION OF POWER COLLECTION DYNAMICS FOR SIMPLY SUPPORTED POWER RAIL

C.H. Spenny
Transportation Systems Center
Kendall Square
Cambridge, Ma. 02142

NOVEMBER 1972

FINAL REPORT

Prepared for:
DEPARTMENT OF TRANSPORTATION
FEDERAL RAILROAD ADMINISTRATION
Office of Research, Development and Demonstration
Washington, D.C. 20590

1. Report No.	2. Government Accession No.	3. Recipient's Catalog No.
FRA-RT-73-15		

4. Title and Subtitle	5. Report Date
SIMULATION OF POWER COLLECTION DYNAMICS FOR SIMPLY SUPPORTED POWER RAIL	NOVEMBER 1972
	6. Performing Organization Code

7. Author(s)	8. Performing Organization Report No.
C.H. Spenny	DOT-TSC-FRA-72-1

9. Performing Organization Name and Address	10. Work Unit No.
Transportation Systems Center Kendall Square Cambridge, MA 02142	R2301
	11. Contract or Grant No. RR205
	13. Type of Report and Period Covered JULY 1971-JUNE 1972 Final Report
12. Sponsoring Agency Name and Address Department of Transportation Federal Railroad Administration Office of Res., Devel. & Demon. Washington, D.C. 20590	14. Sponsoring Agency Code

15. Supplementary Notes

16. Abstract

The mathematical model of a sprung mass moving along a simply supported beam is used to analyze the dynamics of a power-collection system. A computer simulation of one-dimensional motion is used to demonstrate the phenomenon of collector-power rail interaction. Parametric resonance in an undamped collector is shown to exist at several speeds below 300 miles per hour. However, it is demonstrated that amplitude can be controlled at all of these resonant speeds with the proper use of damping.

February 1973

17. Key Words	18. Distribution Statement
Power Collection, High Speed Tracked Vehicles	DOCUMENT IS AVAILABLE TO THE PUBLIC THROUGH THE NATIONAL TECHNICAL INFORMATION SERVICE, SPRINGFIELD, VIRGINIA 22151.

19. Security Classif. (of this report)	20. Security Classif. (of this page)	21. No. of Pages	22. Price
Unclassified	Unclassified	48	

PREFACE

The simulation described in this report was developed in the Power and Propulsion Branch at the Transportation Systems Center (TSC) for the Office of Research, Development and Demonstrations (ORD&D), Federal Railroad Administration. The objective of this work was to develop a model of captive power collector dynamics, to determine the basic dynamic characteristics and to examine the possibility for interaction between the collector and power rail.

The simulation work was performed at the TSC's hybrid computing facility with the assistance of Mr. George Eddleston of Kentron Hawaii, Ltd. Technical advice was provided by Professor David Wormley of MIT whose model of vehicle-guideway dynamics was extended to the power collection problem. Data on the power collection system being developed for the ORD&D tracked air cushion research vehicle was supplied by the Air Research Manufacturing Company, a Division of the Garrett Corporation.

TABLE OF CONTENTS

LIST OF ILLUSTRATIONS

LIST OF TABLES

1.0 INTRODUCTION

Power collection for high speed tracked air cushion vehicles (TACV's) requires considerably more design attention than it has been given in the past. Large vehicle motions relative to the collector rail, inertial forces that increase with the square of vehicle speed, and increased power transfer requirements are major factors which make collector dynamics a significant design problem.

To indicate how critical the dynamic problem can be, consider a 10 pound brush assembly traveling at 300 mph on rail supported at 10 foot intervals. If there is a .05" deflection between supports (which is rather small and could result from sag, for example), then a preload of 50 pounds is required to maintain contact with the rail. Such forces can cause rail deflections even larger than those of sag due to rail weight, and thereby provide the mechanism for the occurrence of rail-collector interaction which is similar to that of a vehicle traveling on a flexible guideway. This problem has not appeared in any low speed applications to date, but is considered a serious problem at the 300 mph speed which the tracked air cushion research vehicle (TACRV) is capable of achieving.

2.0 COLLECTOR DYNAMICS

At low speeds, it has been shown that the least brush wear results if brush to rail contact pressure remains constant. The same is probably true at 300 mph. The following analysis shows how a collector system can be tuned so as to maintain constant contact force at some prescribed vehicle speed. Influence of the collector on the rails is neglected. The schematic shown in Figure 1 represents a collector plug which is "constrained" against lateral motion while traveling between two rails whose shapes are prescribed for constant speed, v, as sine waves.

$$Y_1(t) = Y_2(t) = A\left[1-\cos\left(2\pi\frac{v}{\ell}\cdot t\right)\right] \tag{1}$$

where

$2A$ = amplitude of rail sag

ℓ = spacing between rail supports

The equation of vertical motion for the collector M_c, can be written (assuming the brushes maintain contact with the rail) as:

$$M_c\ddot{Y}_c + 2K\,Y_c - K\left(Y_1 + Y_2\right) = 0 \tag{2}$$

where

M_c = collector body mass

K = spring constant between collector body and brush

With Equation (1) inserted into Equation (2), the steady state solution is:

$$Y_c = A\left[1 - \frac{2K}{2K-\omega^2 M_c}\cdot\cos\omega t\right] \tag{3}$$

where

$$\omega = 2\pi\frac{v}{\ell}.$$

The brush to rail contact force can then be calculated. Due to symmetry, only one of the two brush to rail contact forces need be considered.

$$F_{c_1} = +\frac{K\omega^2 M_c\, A\cos\omega t}{2K-\omega^2 M_c} + P_0 + m_b\omega^2 A\cos\omega t \tag{4}$$

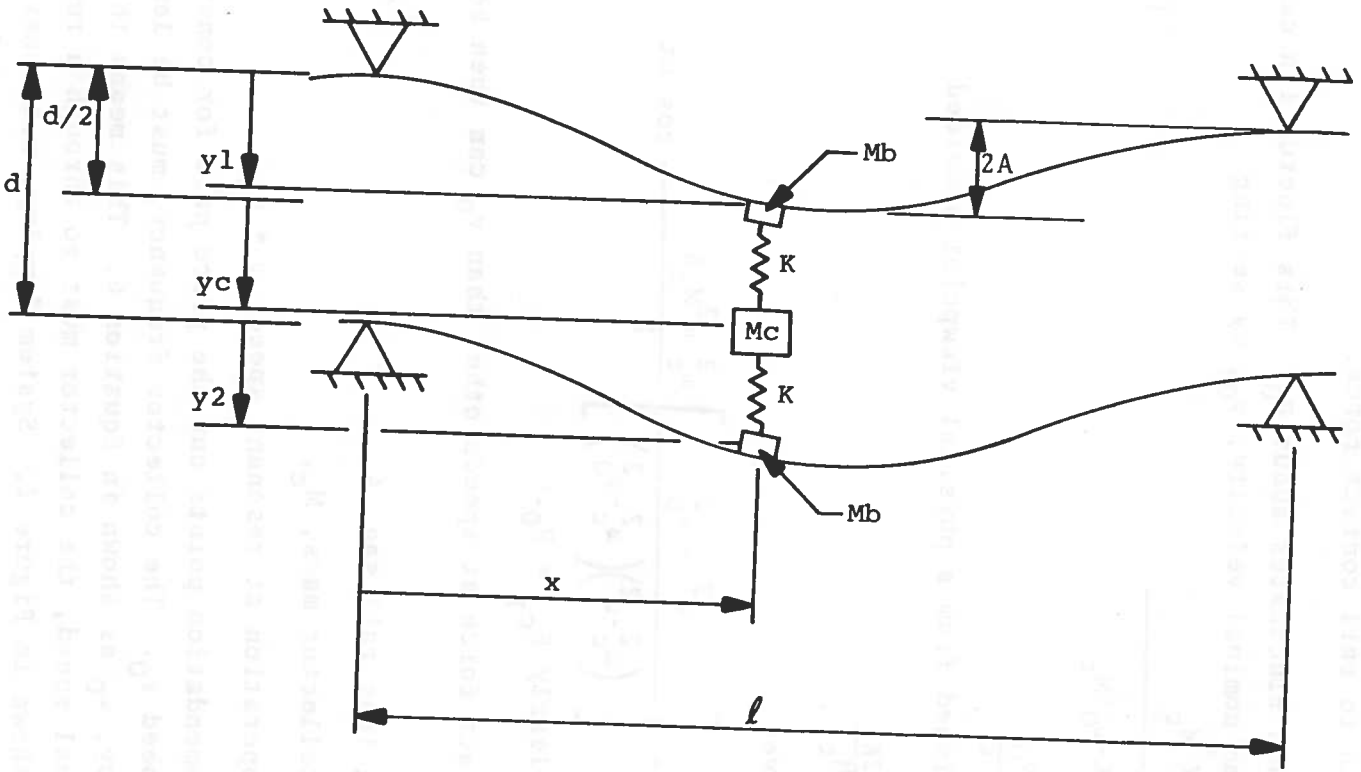

Figure 1 - Model of Rail and Captive Collector

where

P_0 = preload in two springs

F_{c_1} = brush to rail contact force.

The contact force then fluctuates about P_0. This fluctuation can be eliminated at some nominal velocity, v_0, by setting

$$m_b = - \frac{K M_c}{2K - \omega_0^2 M_c} \tag{5}$$

where $\omega_o = 2 \pi \frac{v_0}{\ell}$.

This can be accomplished from a physical viewpoint provided

$$\omega_0^2 > \omega_c^2 = \frac{2K}{M_c} . \tag{6}$$

Then, Equation 4 gives

$$F_{c_1} = P_0 + \left[\frac{\omega^2 - \omega_0^2}{\left(\omega_c^2 - \omega^2\right)\left(\omega_c^2 - \omega_0^2\right)} \right] \frac{\omega_c^2 \omega^2 M_c A}{2} \cos \omega t \tag{7}$$

at speed, $v = v_0$, clearly $F_{c_1} = P_0$.

Fluctuation in contact force at speeds other than v_0 can then be minimized by

1. permitting less rail sag, A,
2. reducing collector mass, M_c,
3. avoiding operation at resonant speed, $\omega = \omega_c$.

The last recommendation points out the price paid for constant contact force at speed v_0. The collector frequency, must be less than speed frequency, ω_0 as shown in Equation 6. This means that on the way up to nominal speed, the collector must go through a resonant frequency as shown in Figure 2. System damping, not considered here, will hold the amplitude to a finite value at resonant frequency. Choice of ω_c at a frequency corresponding to an "unused" vehicle speed is recommended.

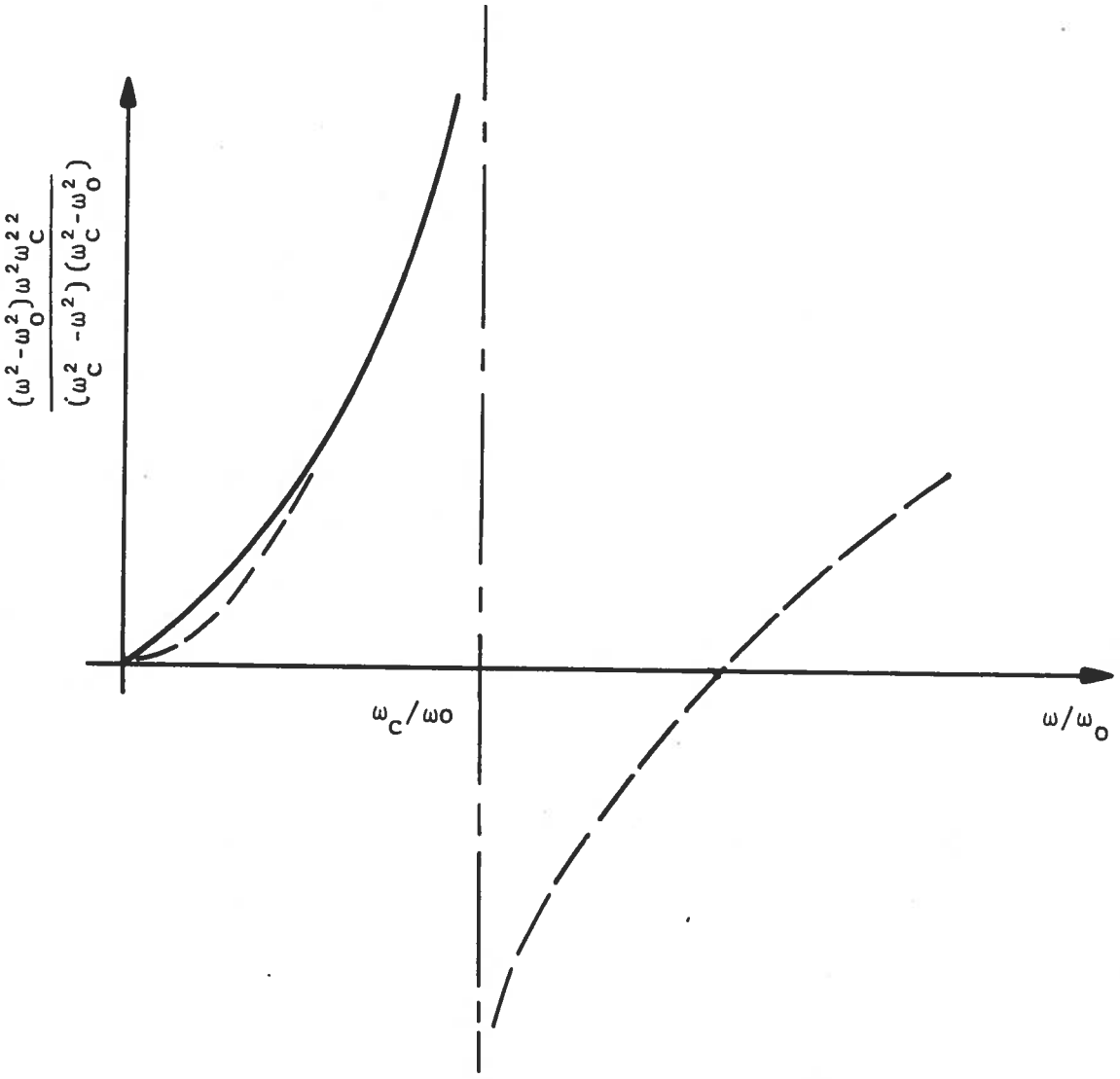

Figure 2 - Frequency Response of Collector

Fluctuation in brush pressure can also be reduced by increasing the brush area while maintaining the same brush mass.

3.0 COLLECTOR-RAIL INTERACTION

The analysis in the preceding section assumed the collector did not exert significant forces against the rail. The example cited in the introduction has, however, shown that there is a mechanism for collector and rail interaction.

The model of Figure 1 can be used to simulate in one dimension, a collector of the type used on the French Aerotrain. The application of a preload between the collector and each rail is such that the upper and lower rails tend to separate. Such is not the case in the TACRV configuration, as seen in Figure 3 where the brushes are opposed or "dual facing" so that preload applies no net force to the rails. However, if one neglects the influence of the brush mass on rail and collector motions and assumes that the brushes do not separate from the rail, equations developed from the model shown in Figure 1 can be used to analyze either configuration. Rail-brush pressure can be calculated separately after the collector and rail equations of motion have been integrated.

The equations of motion of a collector body and the pair of simply supported rail sections that contain the collector are derived below. The technique is similar to that used by Chiu, et al[1] in analyzing rail-vehicle interactions.

Using the notation defined by Figure 1, the equation of motion of the collector for continuous brush contact is

$$M_c(\ddot{Y}_c - \alpha g) + C_1(\dot{Y}_c - \dot{Y}_{1c}) + C_2(\dot{Y}_c - \dot{Y}_{2c}) + K_1(Y_c - Y_{1c}) + K_2(Y_c - Y_{2c}) = 0 \qquad (8)$$

where $M_c\,\alpha g$ is that portion of the collector weight not supported by the vehicle through a pantograph (pantograph dynamics and vehicle induced motions have not been included) and

$$Y_{ic} \equiv Y_i(X_c, t). \qquad i = 1,2$$

Rail motion is given by the Bernoulli-Euler partial differential equation,

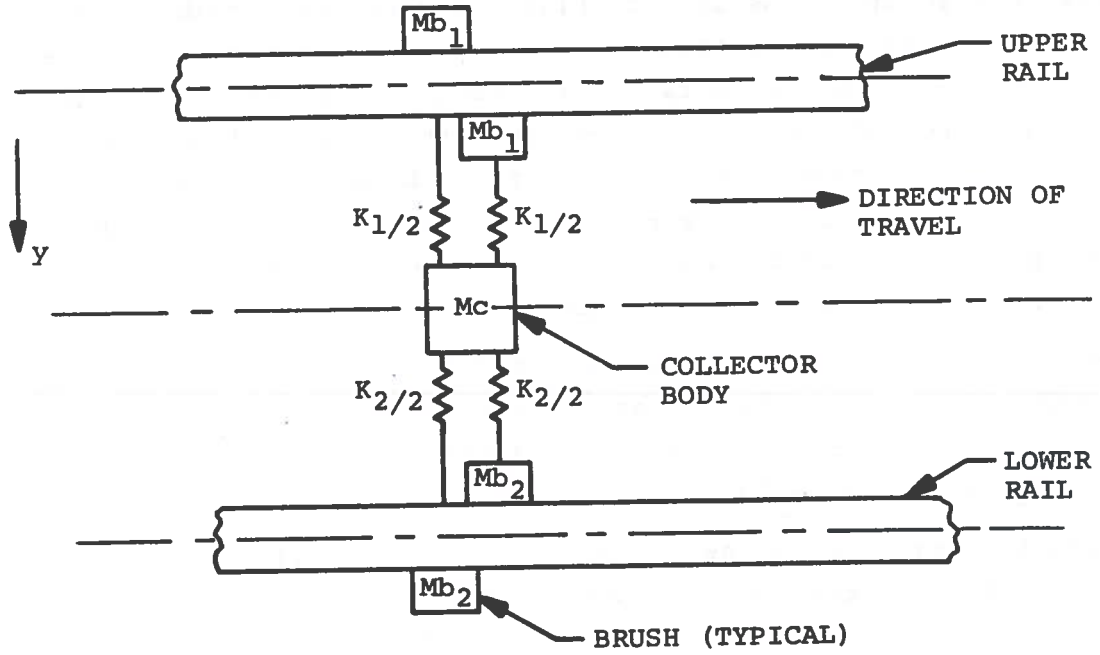

Figure 3-One Dimensional Model of the TACRV Collector and Rail

$$E_i I_i \ell \frac{\partial^4 Y_i}{\partial x^4} + \rho_i a_i \ell \frac{\partial^2 Y_l}{\partial t^2} + C_{ri} \frac{\partial Y_i}{\partial t} = F_i(x,t) + \rho_i a_i \ell g \qquad i=1,2 \qquad (9)$$

where

E_i = elastic modulus of $i^{\underline{th}}$ rail

I_i = $i^{\underline{th}}$ rail moment of inertia

ρ_i = $i^{\underline{th}}$ rail mass density

a_i = $i^{\underline{th}}$ rail cross-sectional area

C_{ri} = $i^{\underline{th}}$ rail damping

$F_i(x,t)$ = force exerted on $i^{\underline{th}}$ rail.

Boundary conditions for a rail that is broken at each support are

$$Y_i(0,t) = Y_i(\ell,t) = \frac{\partial^2 Yi(0,t)}{\partial x^2} = \frac{\partial^2 Y_i(\ell,t)}{\partial x^2} = 0 \qquad (10)$$

Initial conditions can be specified for any amount of rail sag. For example, the equations for the deflection of a simply supported beam due to its weight are given by

$$Y_i(x,0) = \frac{\rho_i a_i x}{24 E_i I_i} (\ell^3 - 2\ell x^2 + x^3)$$

$$\frac{\partial Yi}{\partial x}(x,0) = \frac{\rho_i a_i}{24 E_i I_i} (\ell^3 - 6\ell x^2 + 4x^3) \qquad (11)$$

Using the modal method to solve Equation 9, let

$$Y_i(x,t) = \sum_{n=1}^{\infty} A_{in}(t)\, \phi_n(x) \qquad (12)$$

where orthogonality of modes is imposed by

$$\int_0^{\ell} \phi_n(x)\ \phi_j\ (x)dx = \begin{cases} \ell/2, & j = n \\ 0\ , & j \neq n \end{cases} \tag{13}$$

Assuming a solution of the form $\phi_n(x) = \sin \frac{n\pi x}{\ell}$, substitute Equation 12 into Equation 9 and impose Equation 13 to obtain the ordinary differential equations describing modal amplitudes, A_{in},

$$\ddot{A}_{in} + \frac{b_{in}}{\rho_i a_i \ell}\ \dot{A}_{in} + \omega_{in}^2\ A_{in} = \frac{2}{\rho_i a_i \ell^2} \cdot \int_0^{\ell} F_i(x,t)\ \sin \frac{n\pi x}{\ell}\ dx$$

$$+ \begin{cases} 0 & n = \text{even} \\ \frac{4g}{n\pi} & n = \text{odd} \end{cases} \tag{14}$$

where

$$\omega_{in} = \frac{n^2\pi^2}{\ell^2} \sqrt{\frac{E_i I_i}{\rho_i a_i}}\ .\ i = 1,\ 2$$

b_{in} = damping in i^{th} rail, n^{th} mode.

Assume the only force besides gravity acting on the rails is caused by the collector.

Then,

$$F_i(x,t) = F_i(x_c,t) = f_i(t)\ \delta(\frac{x}{\ell} - \frac{vt}{\ell}) \tag{15}$$

where

v = vehicle speed

$$\delta = \begin{cases} 1 & x/\ell = \frac{vt}{\ell} \leq 1 \\ 0 & x/\ell \neq \frac{vt}{\ell} \text{ or } \frac{vt}{\ell} > 1 \end{cases}$$

Observe that $\frac{2}{\rho a \ell} 2 \int_0^{\ell} F_i \sin \frac{n\pi x}{\ell} \, dx = \frac{2}{\rho a \ell} \int_0^{\ell} f_i \, \delta\left(\frac{x}{\ell} - \frac{vt}{\ell}\right) \sin \frac{n\pi x}{\ell} \, \frac{dx}{\ell}$

$$= \frac{2}{\rho a \ell} f_i \sin \frac{n\pi vt}{\ell}$$

and Equation 14 becomes, for a vehicle traveling at constant speed

$$\ddot{A}_{in} + \frac{b_{in}}{\rho_i a_i \ell} \dot{A}_{in} + \omega_{in}^2 A_{in} = \frac{2\delta \, f_i(t)}{\rho_i a_i \ell} \sin \frac{n \, \pi \, vt}{\ell} \qquad (16)$$

$$+ \begin{cases} 0 & n = \text{even} \\ \frac{4g}{n\pi} & n = \text{odd} \end{cases}$$

where the definition of the delta function is now reduced to

$$\delta = \begin{cases} 1, \; vt/\ell \leq 1 & \text{load on the span} \\ 0, \; vt/\ell > 1 & \text{load off the span} \end{cases}$$

The force exerted on each rail by the collector can be expressed, neglecting the acceleration of the brush mass, as

$$f_i \, (t) = K_i \, (Y_c - Y_{ic}) + C_i \, (\dot{Y}_c - \dot{Y}_{ic}) \mp P_0 \qquad (17)$$

where P_0 = preload at x = 0 and the negative sign applies for i = 1, positive sign for i = 2. Equation 16 then becomes

$$\ddot{A}_{in} + \frac{b_{in}}{\rho_i a_i \ell} \dot{A}_{in} + \omega_{in} A_{in} = \frac{2 \, \delta}{\rho_i a_i \ell} \left[K_i \, (Y_c - Y_{ic}) \right. \qquad (18)$$

$$\left. + C_i \, (\dot{Y}_c - \dot{Y}_{ic}) \mp P_0 \right] \sin \frac{n \, \pi \, vt}{\ell} + \begin{cases} 0 & n = \text{even} \\ \frac{4g}{n\pi} & n = \text{odd} \end{cases}$$

Equations 8 and 18 are 2n + 1 differential equations which completely describe the motion of the collector and the motion of the upper and lower rail spans between the two supports which contain the collector.

4.0 ANALOG SIMULATION

Since it has been assumed that the rails are simply supported, there are no moments transmitted from one span to the next and it is not necessary to look at rail motion ahead of the particular span which contains the collector. Rail damping causes motion in spans which have already been traversed to decay rapidly. Therefore, it is sufficient to examine only the span in which the collector is located to find maximum rail displacements. Considering only the first mode for each rail and eliminating Y_{ic} from Equations 8 and 18 using Equation 12, the three coupled second order differential equations which completely discribe rail and collector motion are:

upper rail,

$$\ddot{A}_{11} = -\left[2\xi_1\omega_{11} + \frac{2C_1}{\rho_1 a_1 \ell}\sin^2\left(\frac{\pi vt}{\ell}\right)\right]\dot{A}_{11} \tag{19}$$

$$-\left[\omega_{11}^2 + \frac{2K_1}{\rho_1 a_1 \ell}\sin^2\left(\frac{\pi vt}{\ell}\right)\right]A_{11}$$

$$+\left[\frac{2C_1}{\rho_1 a_1 \ell}\left|\sin\left(\frac{\pi vt}{\ell}\right)\right|\right]\dot{Y}_c + \left[\frac{2K_1}{\rho_1 a_1 \ell}\left|\sin\left(\frac{\pi vt}{\ell}\right)\right|\right]Y_c$$

$$+\frac{4g}{\pi} - \frac{2P_o}{\rho_1 a_1 \ell}\left|\sin\left(\frac{\pi vt}{\ell}\right)\right|$$

collector,

$$\ddot{Y}_c = -2\left(\xi_{c1}\,\omega_{c1} + \xi_{c2}\,\omega_{c2}\right)\dot{Y}_c - \left(\omega_{c1}^2 + \omega_{c2}^2\right)Y_c \qquad (20)$$

$$+\left[2\xi_{c1}\,\omega_{c1}\left|\sin\left(\frac{\pi vt}{\ell}\right)\right|\right]\dot{A}_{11} + \left[2\xi_{c2}\,\omega_{c2}\left|\sin\left(\frac{\pi vt}{\ell}\right)\right|\right]\dot{A}_{21}$$

$$+\left[\omega_{c1}^2\left|\sin\left(\frac{\pi vt}{\ell}\right)\right|\right]A_{11} + \left[\omega_{c2}^2\left|\sin\left(\frac{\pi vt}{\ell}\right)\right|\right]A_{21} + \alpha g$$

lower rail,

$$\ddot{A}_{21} = -\left[2\xi_2\,\omega_{21} + \frac{2C_2}{\rho_2 a_2 \ell}\sin^2\left(\frac{\pi vt}{\ell}\right)\right]\dot{A}_{21} \qquad (21)$$

$$-\left[\omega_{21}^2 + \frac{2K_2}{\rho_2 a_2 \ell}\sin^2\left(\frac{\pi vt}{\ell}\right)\right]A_{21}$$

$$+\left[\frac{2C_2}{\rho_2 a_2 \ell}\left|\sin\left(\frac{\pi vt}{\ell}\right)\right|\right]\dot{Y}_c + \left[\frac{2K_2}{\rho_2 a_2 \ell}\left|\sin\left(\frac{\pi vt}{\ell}\right)\right|\right]Y_c$$

$$+\frac{4g}{\pi} + \frac{2P_o}{\rho_2 a_2 \ell}\left|\sin\left(\frac{\pi vt}{\ell}\right)\right|$$

where

$$\xi_i = \frac{b_{i1}}{2\rho_i a_i \ell \omega_{i1}}$$

$$\omega_{ci} = \sqrt{K_i/M_c}$$

$$\xi_{ci} = C_i/2M_c\omega_{ci}$$

To compute actual rail displacement at any point, A_{i1} obtained from the above equations is inserted in Equation 12,

$$Y_i(x,t) = A_{i1}(t) \sin\left(\frac{\pi v t}{\ell}\right). \tag{22}$$

Note the only periodic forcing function capable of driving Equations 19 - 21 is the preload term, $\frac{P_{o1}}{\rho_i a_i \ell} \left| \sin \frac{\pi v t}{\ell} \right|$, which is non-zero only for the single sided brush configuration. However, the gravity constants for unsupported collector weight, αg, and rail sag, $\frac{4g}{\pi}$, produce static deflections which in turn produce nonzero periodic coefficients in the equations. Thus, parametric excitation with the associated instabilities can occur for both the single sided and the dual facing brush configurations. A computer simulation was developed to examine resonant conditions in the speed range 0-300 miles per hour. Aerodynamic forces and vehicle induced forces acting upon the collector have not been included in this model, but represent additional driving terms to be examined.

Figure 4 is a computer diagram of the analog simulation for Equations 19 - 21*. Preload is set with pots 60 and 160. Unsupported collector weight is prescribed by setting initial conditions on collector displacement and velocity with pots 30 and 31 that are compatible with the constant acceleration set with pot 04. Rail sag is likewise prescribed using pots 26, 27, 124, 34, 35, and 46. As the collector leaves each simply supported rail span, the initial conditions on rail mode shapes must be reset. On an analog computer this can be achieved by putting the collector circuitry in "hold" while resetting the rail initial conditions or by switching in alternate rail circuitry as the collector enters each new span. The latter technique is used in this simulation although not shown in Figure 4.

---

*The analog simulation was originally set up by the author. Alterations and all data generated for this report have been performed by Mr. George Eddleston of Kentron Hawaii, LTD.

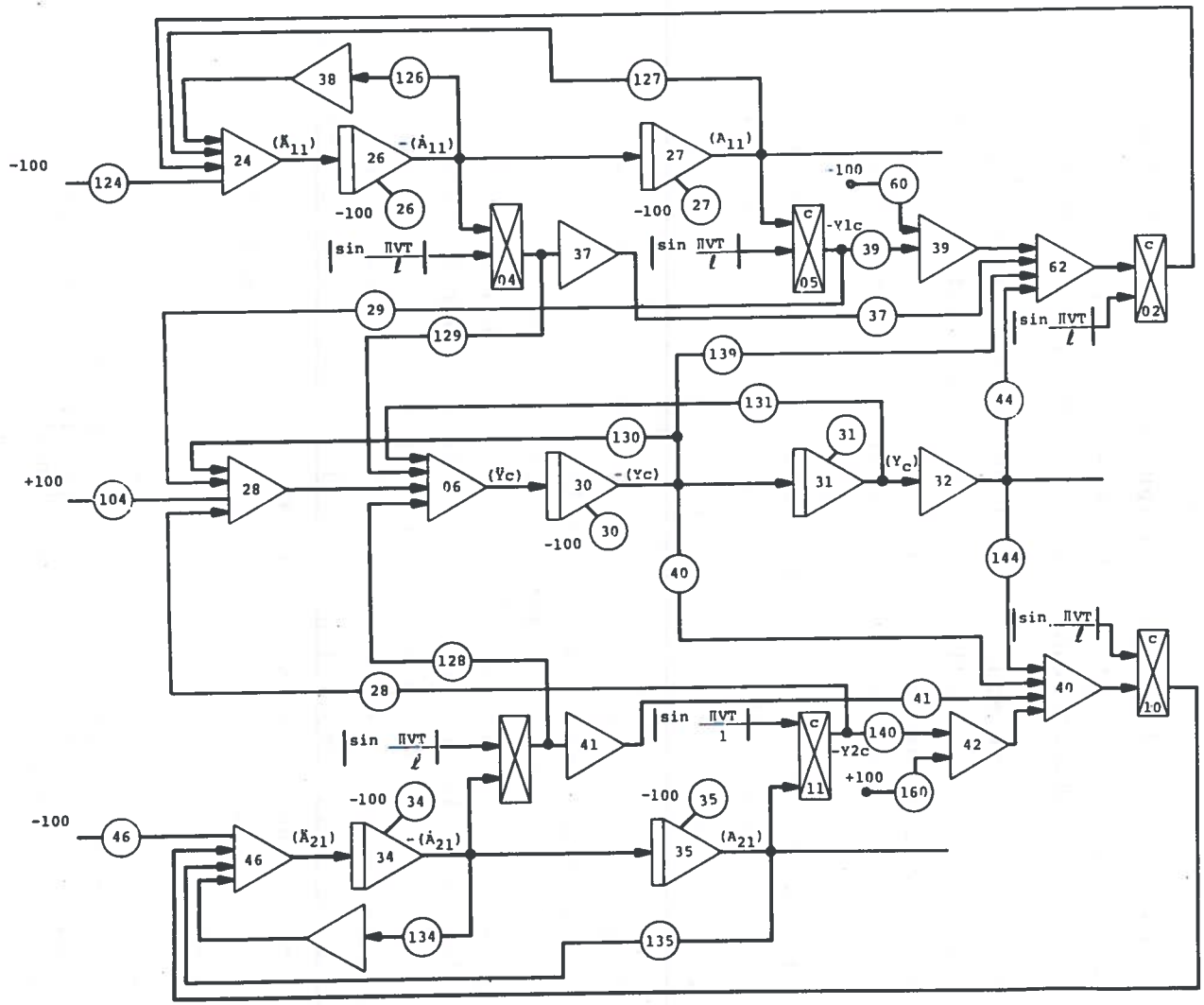

UPPER RAIL	
POT #	VARIABLE
26	$\dot{A}_{11}(0)$
126	$2\xi_1 W_{11}$
127	W_{11}^2
27	$A_{11}(0)$
37	$2c_1/e.a.\ell$
39	$2K_1/e.a.\ell$
60	$2P_0/e.a.\ell$
29	Wc_1^2
129	$2\xi c_1 Wc_1$
124	$4g/\pi$

COLLECTOR	
POT #	VARIABLE
30	$Yc(0)$
130	$2(\xi c_1 Wc_1+\xi c_2 Wc_2)$
131	$Wc_1^2+Wc_2^2$
31	$Yc(0)$
40	$2c_2/e_2a_2\ell$
44	$2K_1/e_1a_1\ell$
144	$2K_2/e_2a_2\ell$
139	$2c_1/e.a.\ell$
04	αg

LOWER RAIL	
POT #	VARIABLE
34	$\dot{A}_{21}(0)$
134	$2\xi_2 W_{21}$
135	W_{21}^2
35	$A_{21}(0)$
128	$2\xi c_2 Wc_2$
41	$2c_2/e_2a_2\ell$
140	$2K_2/e_2a_2\ell$
160	$2P_0/e_2a_2\ell$
28	W^2c_2
46	$4g/\pi$

Figure 4 - Computer Diagram of Collector-Rail Dynamics Simulation

Nominal parameter values used in initial simulation work, are shown in Table 1.

TABLE 1. RAIL-COLLECTOR PARAMETERS

$\omega_{c1} = \omega_{c2} = \sqrt{K_i/M_c} = 27.8$ rad/sec.
$\omega_{11} = \omega_{21} = 100$ rad/sec
$K_1 = K_2 = 200$ lb/inch
$\rho_1 a_1 = \rho_2 a_2 = .0053$ lb-sec^2/inch^2 $\ell = 150$ inches
$\xi_1 = \xi_2 = 0.02$
$\xi_{c1} = 0.0$
$M_c = 0.259$ lb-sec^2/in ($W_c = 100$lb.)
$0 < \frac{\pi v}{\ell} < 70$ rad/sec

Figures 5, 6, and 7 show the time response of the rails and collector to the driving force due to preload, unsupported collector weight, and rail sag, respectively. Speed in each case is 300mph.

Figure 5 shows the response when a preload of 100 lb. applied to the brushes deflects the rails, as occurs in the single sided collector concept used on the French Aerotrain. The average position (i.e. dc time average) of the rails, y_{1c} and y_{2c}, represents an increase in distance between rails as the collector, y_c, remains motionless, and the rails spread. However, lack of symmetry, implemented here by reducing the natural frequency of the upper rail to 1/2 of that of the lower rail, causes the preload to excite the collector at its own natural frequency as shown by Figure 5b. Since this lack of symmetry exists for an actual collector captured in a three rail cross section, the use of dual facing brushes which do not deflect the rails offers the advantage of eliminating a source of collector excitation.

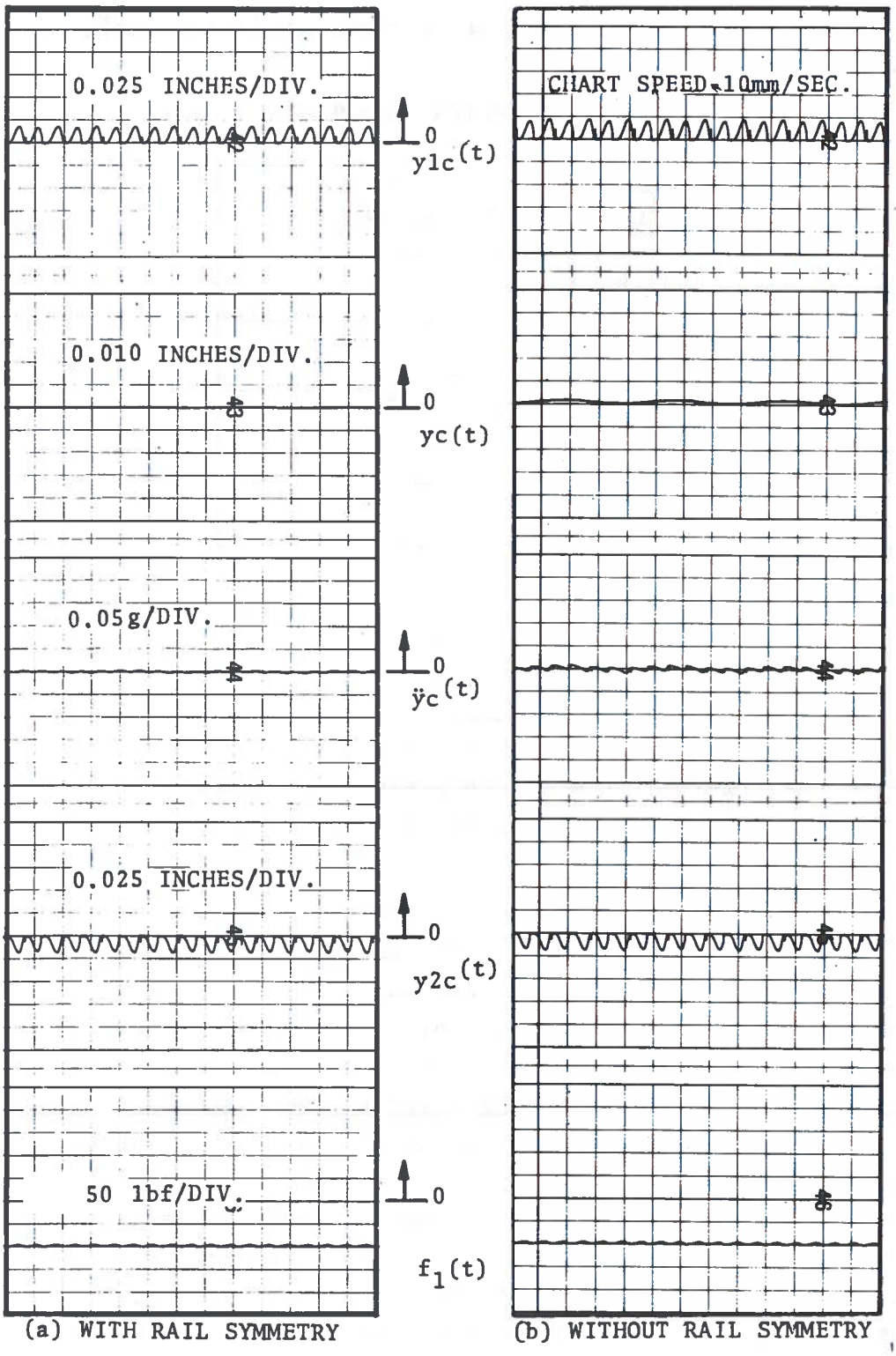

Figure 5 - Time Response of Collector & Rails to Preload

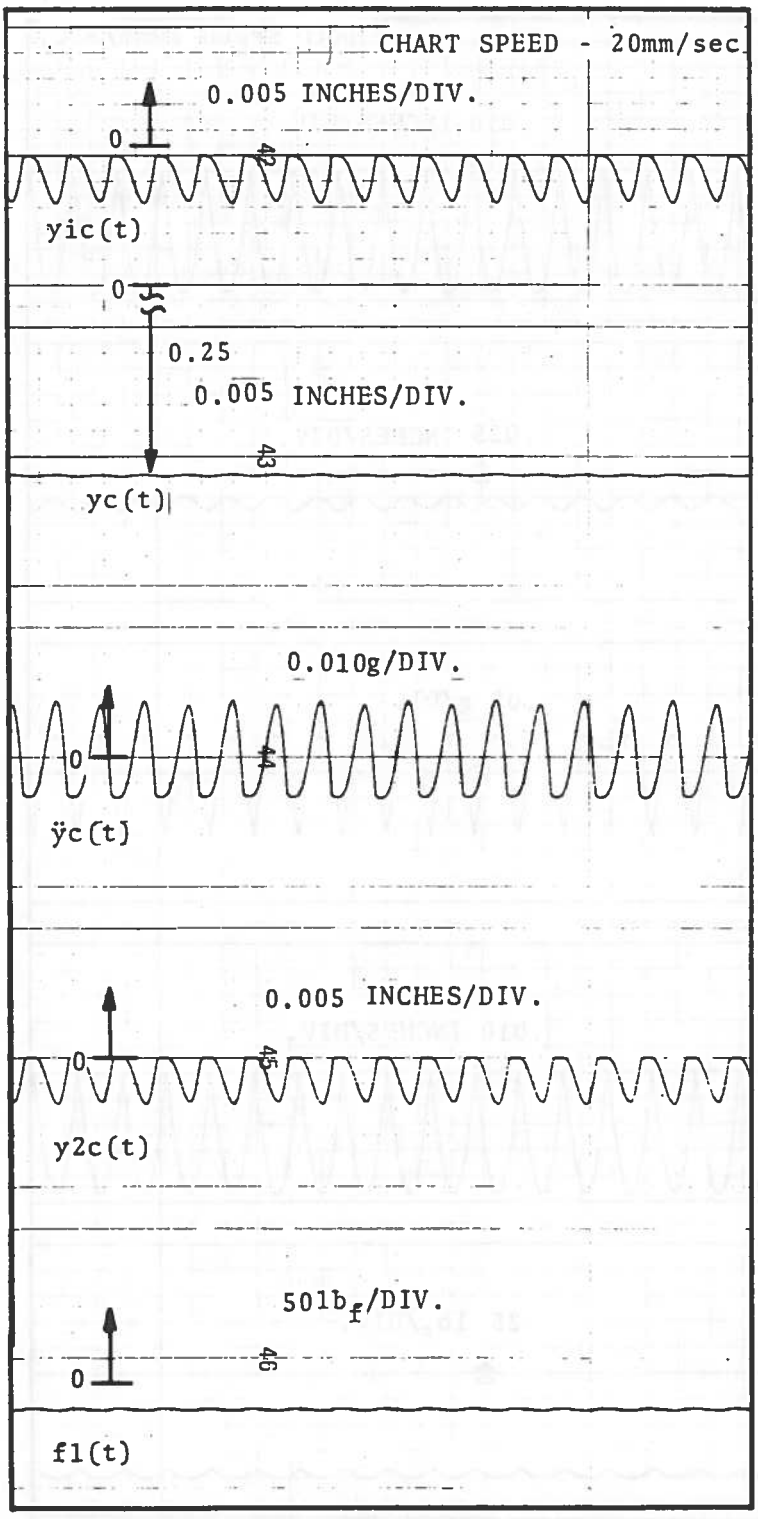

Figure 6 - Time Response of Collector & Rails to Collector Sag

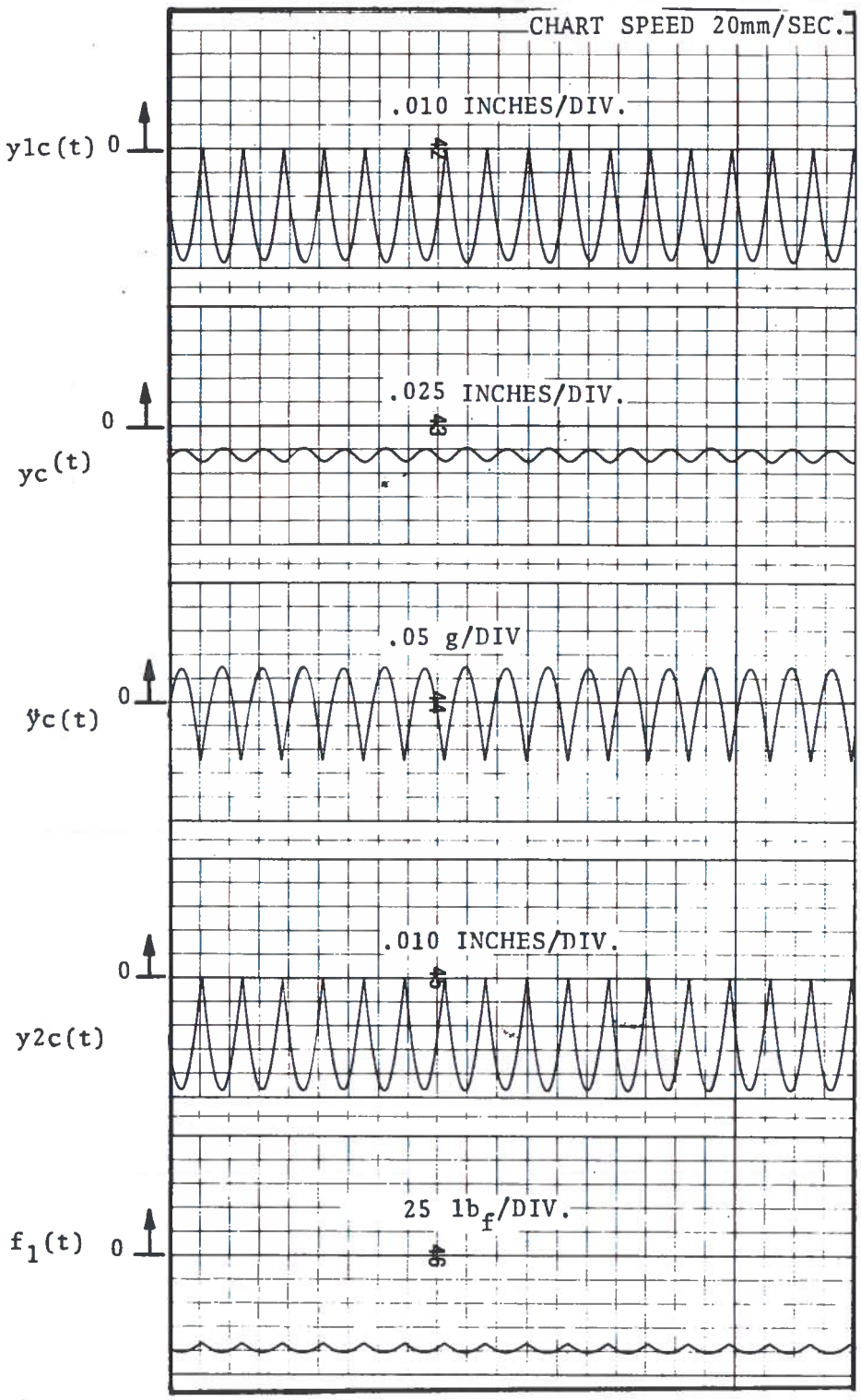

Figure 7 - Time Response of Collector & Rails to Rail Sag

Figure 6 is the case in which all of the collector weight is supported by the rails. The average position of the collector in this case is displaced downward from the midpoint between rails by 1/4 inch; but there is negligible oscillation about this position. Note the rails are both displaced downward. The magnitude of rail oscillation, however, is less than for the previous case. The dc level of brush pressure, $f_1(t)$, of 100 pounds was chosen arbitrarily to demonstrate the fluctuation in brush pressure. Since brush pressure is not deflecting the rails in this and the following cases, these runs simulate the concept of dual facing brushes used on the TACRV.

Figure 7 is the case in which rail sag due to their own weight drives the system. Rail displacement, Y_{ic}, traces half sine waves of nearly equal amplitude which implies that the rail maintains the shape it takes in the static case with rail sag and is essentially undisturbed by collector motions. However, rail sag appears to be the principle exciter of the collector, particularly for the TACRV system where rail deflection due to preload is zero and collector weight is supported by the vehicle through a spring counterbalance. The remainder of this study was made using rail sag to produce collector excitation.

5.0 PARAMETRIC EXCITATION

Equations 19 - 21 can be written in the form of coupled Mathieu equations by applying the trigonometric identity

$$\sin^2 wt = 1/2 - 1/2 \cos 2wt \tag{23}$$

For example, rail motion as defined by Equation 19 becomes

$$\begin{aligned} A_{11} = &- \left[\left(2\xi_1\omega_{11} + \frac{C_1}{\rho_1 a_1 \ell} \right) - \frac{C_1}{\rho_1 a_1 \ell} \cos(2\omega t) \right] \dot{A}_{11} \\ &- \left[\left(\omega_{11}^2 + \frac{K_1}{\rho_1 a_1 \ell} \right) - \frac{K_1}{\rho_1 a_1 \ell} \cos(2\omega t) \right] A_{11} \\ &+ \left[\frac{2C_1}{\rho_1 a_1 \ell} \mid \sin wt \mid \right] \dot{Y}_c + \left[\frac{2K_1}{\rho_1 a_1 \ell} \mid \sin \omega t \mid \right] Y_c \\ &+ \frac{4g}{\pi} \end{aligned} \tag{24}$$

where $P_o = 0$ and $\omega = \frac{\pi v}{\ell}$. Then, letting $\tau = \omega t$, Equation 24 becomes

$$\begin{aligned} \frac{d^2A}{d\tau^2} = &- \frac{1}{\omega} \left[\left(2\xi_1\omega_1 + \frac{C_1}{\rho_1 a_1 \ell} \right) - \frac{C_1}{\rho_1 a_1 \ell} \cos 2\tau \right] \frac{dA_{11}}{d\tau} \\ &- \frac{1}{\omega^2} \left[\left(\omega_{11}^2 + \frac{K_1}{\rho_1 a_1 \ell} \right) - \frac{K_1}{\rho_1 a_1 \ell} \cos 2\tau \right] .A_{11} \\ &+ \frac{1}{\omega} \left[\frac{2C_1}{\rho_1 a_1 \ell} \mid \sin \tau \mid \right] \frac{dy_c}{d\tau} + \frac{1}{\omega^2} \left[\frac{2K_1}{\rho_1 a_1 \ell} \mid \sin \tau \mid \right] Y_c \\ &+ \frac{4g}{\omega^2 \pi} \end{aligned} \tag{25}$$

The unforced and undamped Mathieu Equation which is usually written in the form

$$\ddot{x} + (a + b \cos 2t)\, x = 0 \qquad (26)$$

has regions in a, b space that are unstable regardless of initial conditions. These are the regions labelled U in Figure 8.

Comparing corresponding terms in Equations 25 and 26, note that vehicle speed, ω appears in both the a and b constants.

$$a = \frac{1}{\omega^2}\left(\omega_{11}^2 + \frac{K_1}{\rho_1 a_1 \ell}\right)$$

$$b = \frac{-1}{\omega^2}\left(\frac{K_1}{\rho_1 a_1 \ell}\right)$$

For the parameters given in Table 1, the range of values which the constant a can take on for vehicle speeds up to 300 miles per hour is

$$0.838 < a < \infty .$$

The speed which corresponds to a=1 is 275mph. The unstable regions at a=4, 9 etc. occur at lower speeds. Thus, one might expect to find vehicle speeds at which Equation 25 would be unstable regardless of the amount of damping. However, this equation only describes the rail motion of a single span during the period in which the collector is in that span, so that the slow build up associated with this Mathieu instability does not have a chance to achieve significant amplitude.

The collector, Equation 20, is also susceptible to parametric excitation and in this case, there is sufficient time for build up of collector amplitude. Identification of a and b in Equation 20 is not so obvious. To indicate the presence of variable spring rate consider two constant coefficient cases: (1) the trigonometric coefficients involving time in Equations 19 - 21 take on their midspan values and (2) the trigonometric coefficients take on their end-of-span values. The latter case implies a complete separation of the equations so that the natural frequencies are simply the collector natural frequency and rail natural frequency. For the nominal parameters given by Table 1, collector natural frequency is $\sqrt{39.3}$ rad/sec and rail natural frequency, ω_{11}, is 100 rad/sec.

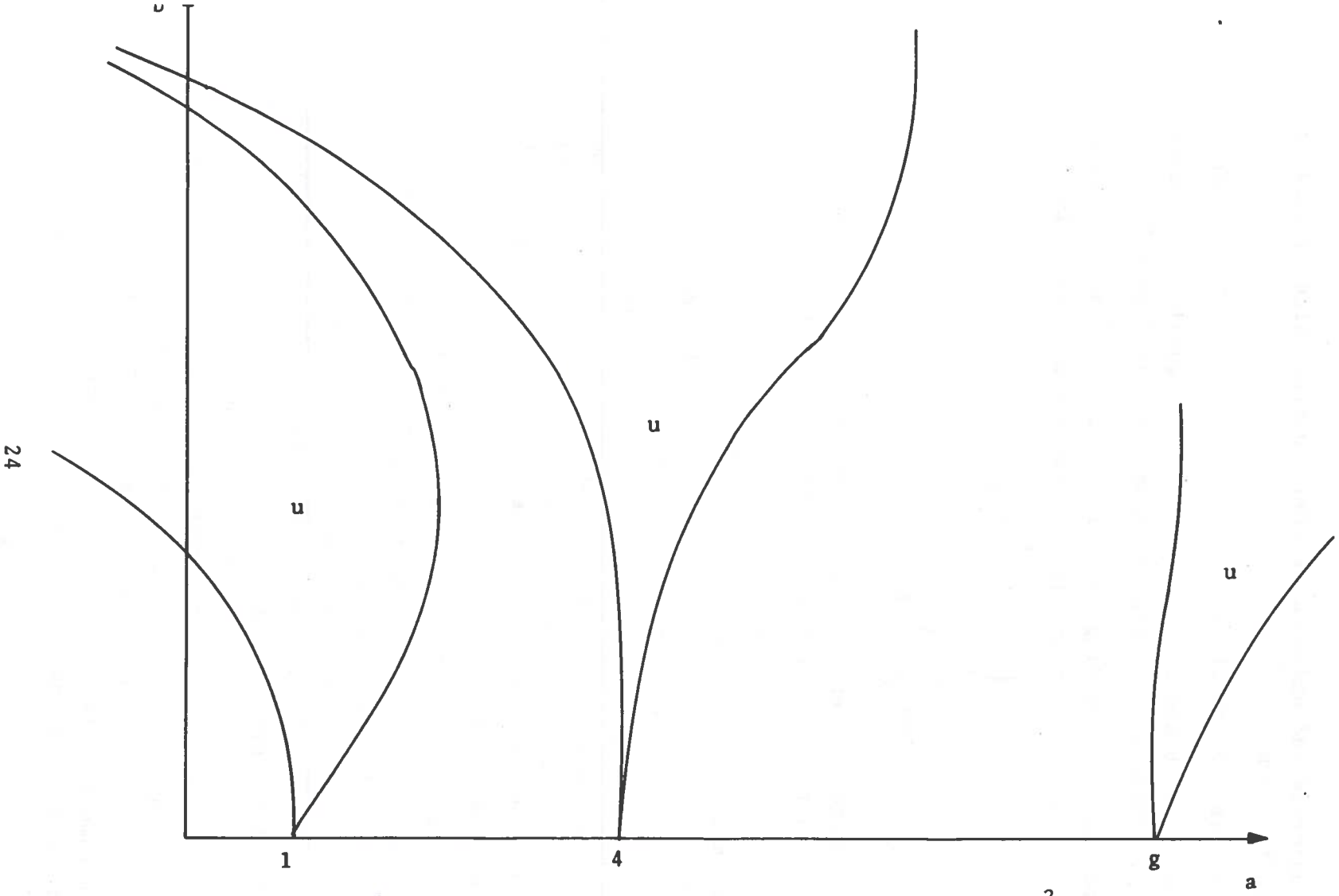

Figure 8 - Instability Regions of Mathieu Equation[2]

For the first case, the equations are coupled but linear so that solution of a cubic characteristic equation yields three eigenvalues, two of which are repeated roots as expected with a pair of identical rails. Again using the values in Table 1, the eigenvalues are $\lambda_1 = 38.2$ rad/sec, $\lambda_2 = \lambda_3 = 102.7$ rad/sec. The two modes of vibration, then, have frequencies of oscillation that vary between the limits

$$38.2 \leq \lambda_1 \leq 39.3 \text{ rad/sec} \tag{27a}$$

$$100 \leq \lambda_2 \leq 102.7 \text{ rad/sec} \tag{27b}$$

or between vehicle speeds

$$103.6 \leq v \leq 106.6 \text{ mph} \tag{28a}$$

$$271.3 \leq v \leq 278.6 \text{ mph} \tag{28b}$$

The speed corresponding to a = 1 of 275 mph is seen to lie midway between the limits given by Equation 28b. Likewise, a low frequency parametric resonance of the collector lies in the speed range given by Equation 28a, and other parametric resonances would be expected at speeds of 1/n times this resonant speed where n = 1, 2, 3.

This has been observed using the computer simulation. "Frequency response" plots as shown in Figures 9 - 11 were generated by running the simulation at many speeds up to 300 mph. The parameter values of Table 1 were used and the excitation was produced by rail sag. The ordinate is the oscillatory component of the parameter plotted. Note in Figure 11 that the ordinate is rail displacement at midspan, A_{i1}, as opposed to displacement under the collector, Y_{ic}, as was plotted in Figures 5 - 7. The dc component average of collector and rail displacements remained constant throughout the speed range. The collector oscillated about a position approximately 0.03" below the equilibrium position. The rail midspan oscillation was about a position approximately 0.05" below the equilibrium position. Rail oscillation is relatively small except at the resonant speeds. At these resonant speeds, the undamped system is unstable. Note the speeds correspond closely with the predicted Mathieu unstable regions for the collector. Not all unstable re-

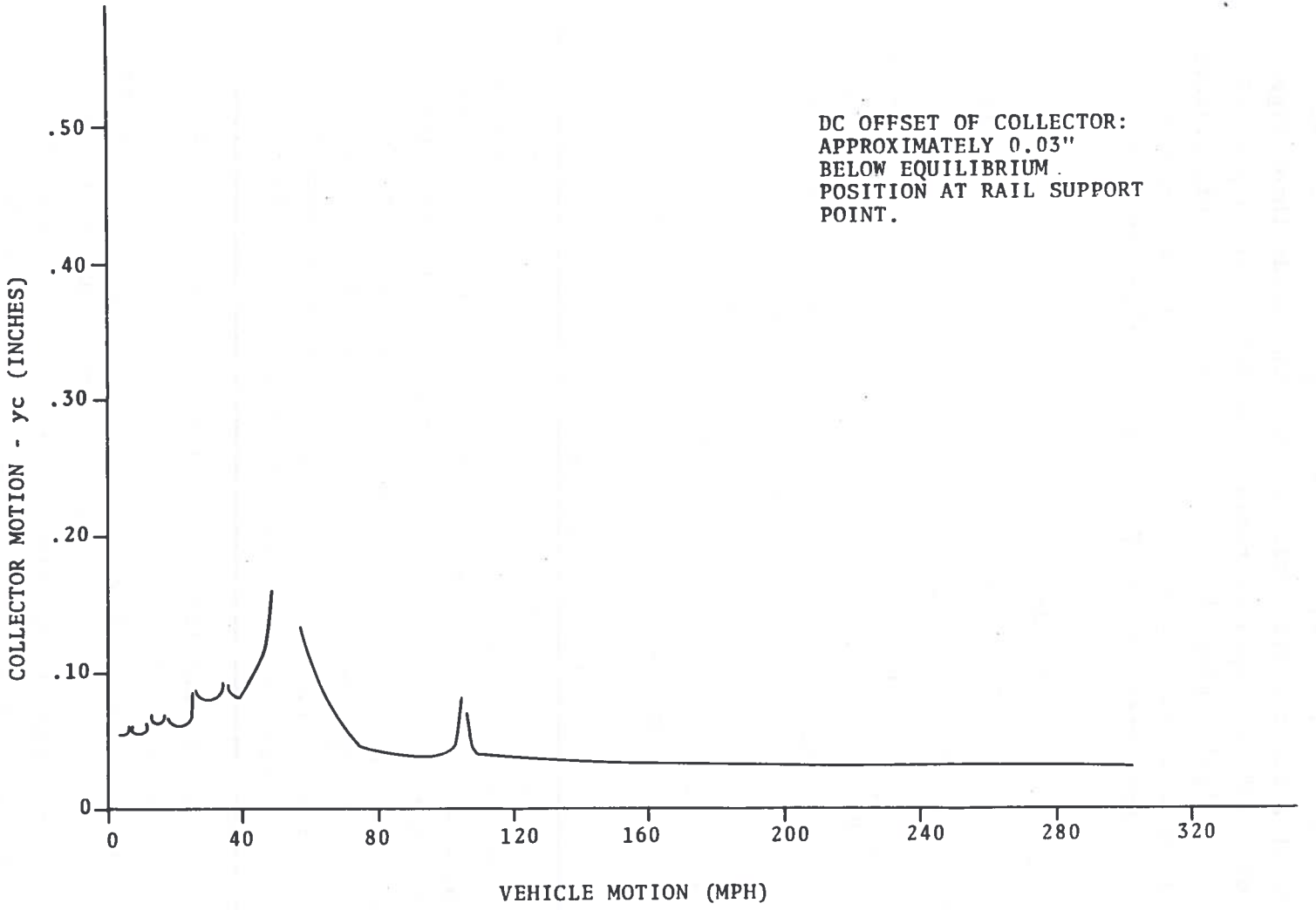

Figure 9 - Collector Oscillation about a dc Offset

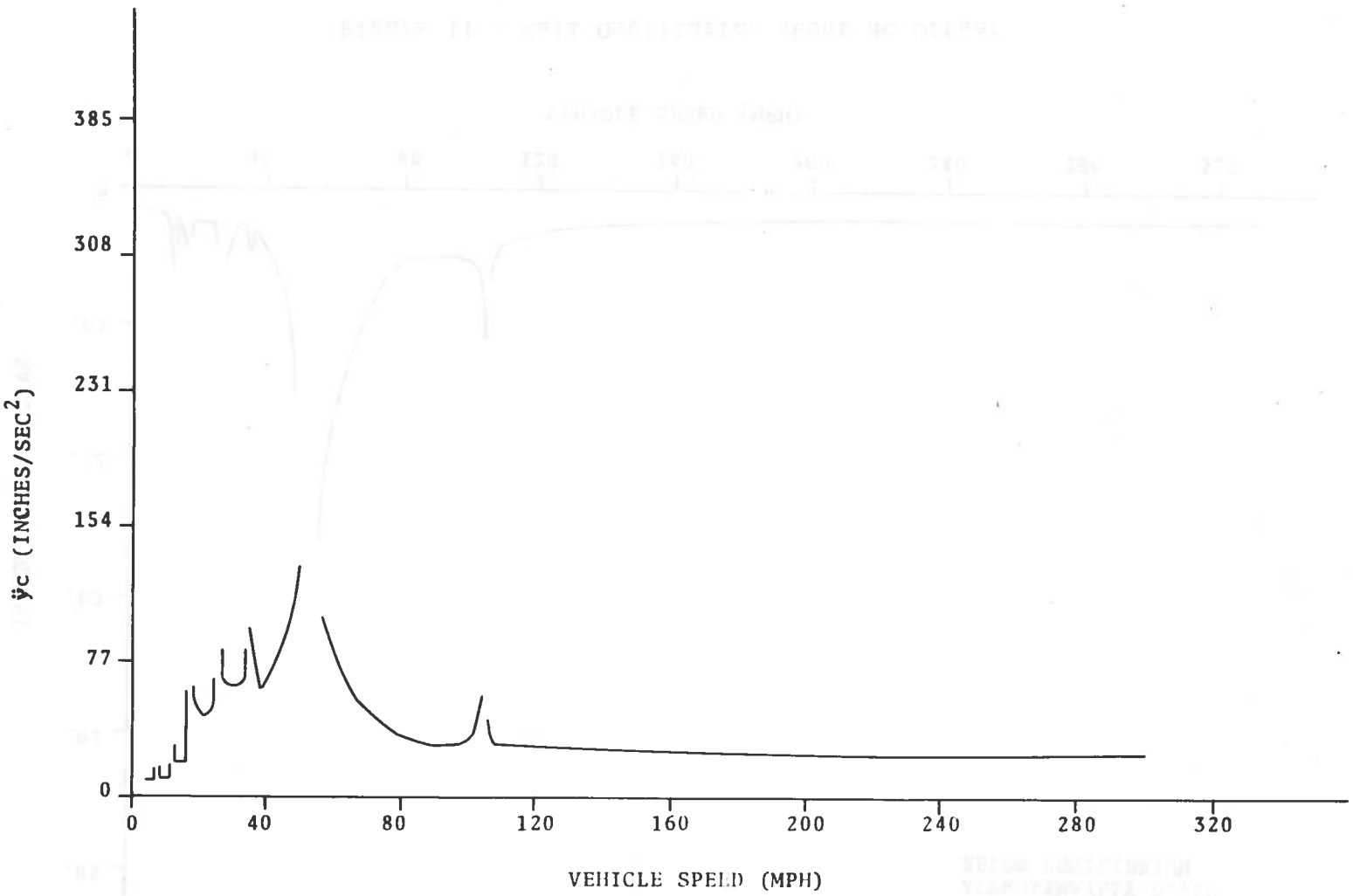

Figure 10 - Collector Acceleration

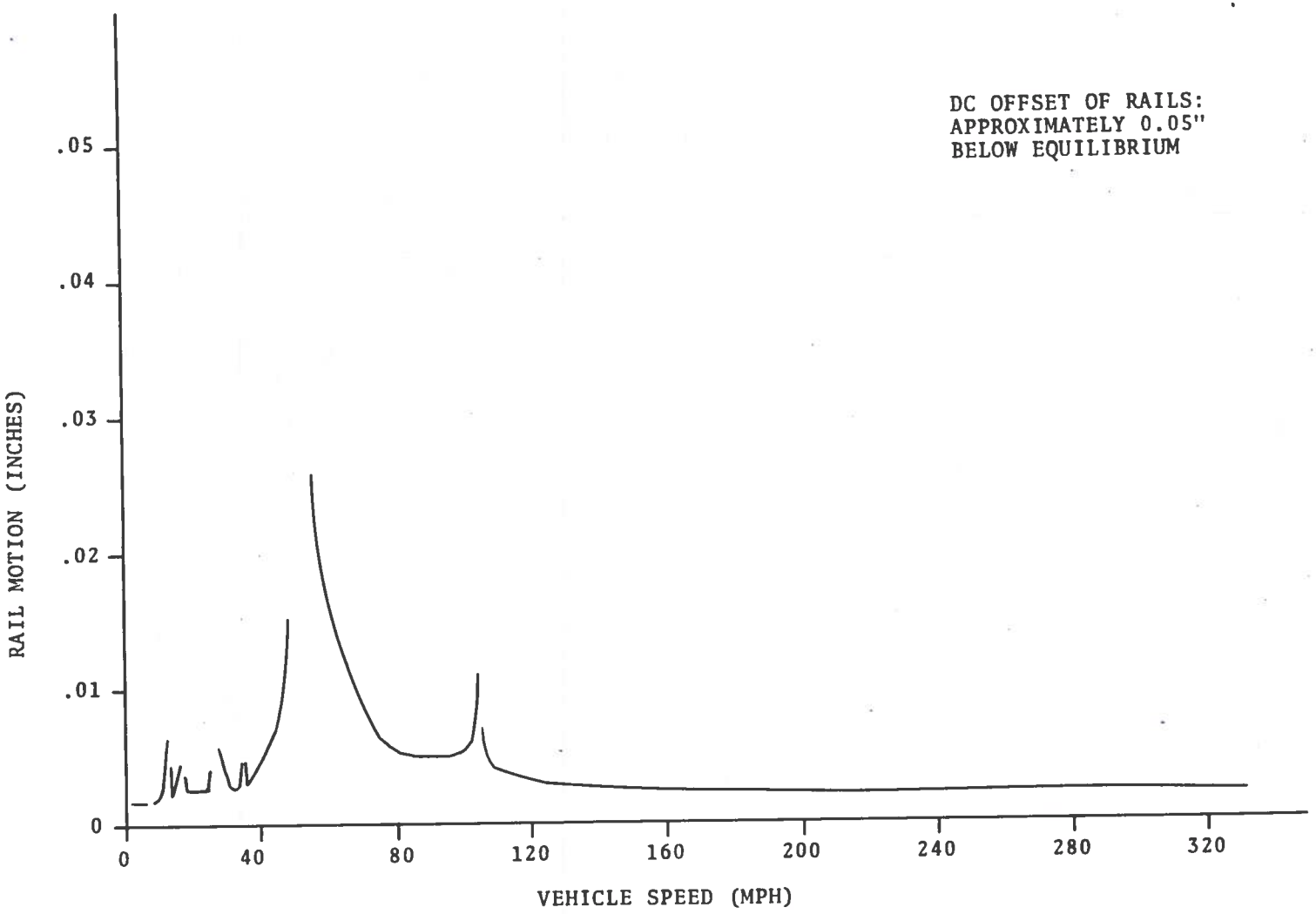

Figure 11 - Rail Oscillation about dc Offset

gions were located, since there are an infinite number as speed approaches zero. No instability at rail resonant speed was detectable because of the limited buildup time. It may be possible to find rail resonance by studying the continuous or welded rail case where collector excitation of the rail is for more than one.

The addition of rail damping alone does not eliminate collector resonance. However, the addition of damping between the collector and brushes or between the collector and vehicle does eliminate collector resonance for speeds up to 300 mph on a simply supported power rail. This would not be expected if the equations were true Mathieu equations since the addition of damping does not eliminate a parametric instability but only reduces the rate at which amplitudes grow. Resetting initial conditions on the two rail modal equations, Equations 19 and 21, appears to alter the dynamics such that true Mathieu behavior does not exist. In any case, these resonances should not be a problem since they occur over very narrow speed ranges that would not be maintained for long periods of time.

6.0 PARAMETRIC STUDY

By changing spring rates and mass of the collector and/or rail, it is possible to change the resonance speeds and the response amplitudes in order to optimize response characteristics and performance parameters such as brush wear and bounce, and collector drag. A thorough optimization has not been undertaken for this report. However, the parameters as shown in Table 1 have been varied from their nominal values, one at a time, to illustrate the effect on resonant speed. Table 2 lists the parametric changes made. Figures 12 - 15 show the shift in collector resonant frequency for each of the parameters varied. Span length and rail natural frequency are seen to have little effect while collector spring rate and collector weight can make significant changes in resonant speed. This indicates the rail parameters have little effect on collector behavior.

TABLE 2. PARAMETRIC VARIATIONS MADE IN STUDY

PARAMETER	SYMBOL	UNITS	VALUES*
Rail Natural Frequency (First Mode)	ω_{11}, ω_{21}	rad/sec	50, 100, 125, 150
Collector to Brush Spring Rate	K_1, K_2	lb/in	100, 200, 350, 500
Collector Weight	M_{cg}	lb.	80, 100, 120, 150
Rail Span Length	ℓ	ft.	10, 12.5, 15, 20

*Values in boxes represent nominal case of Table 1.

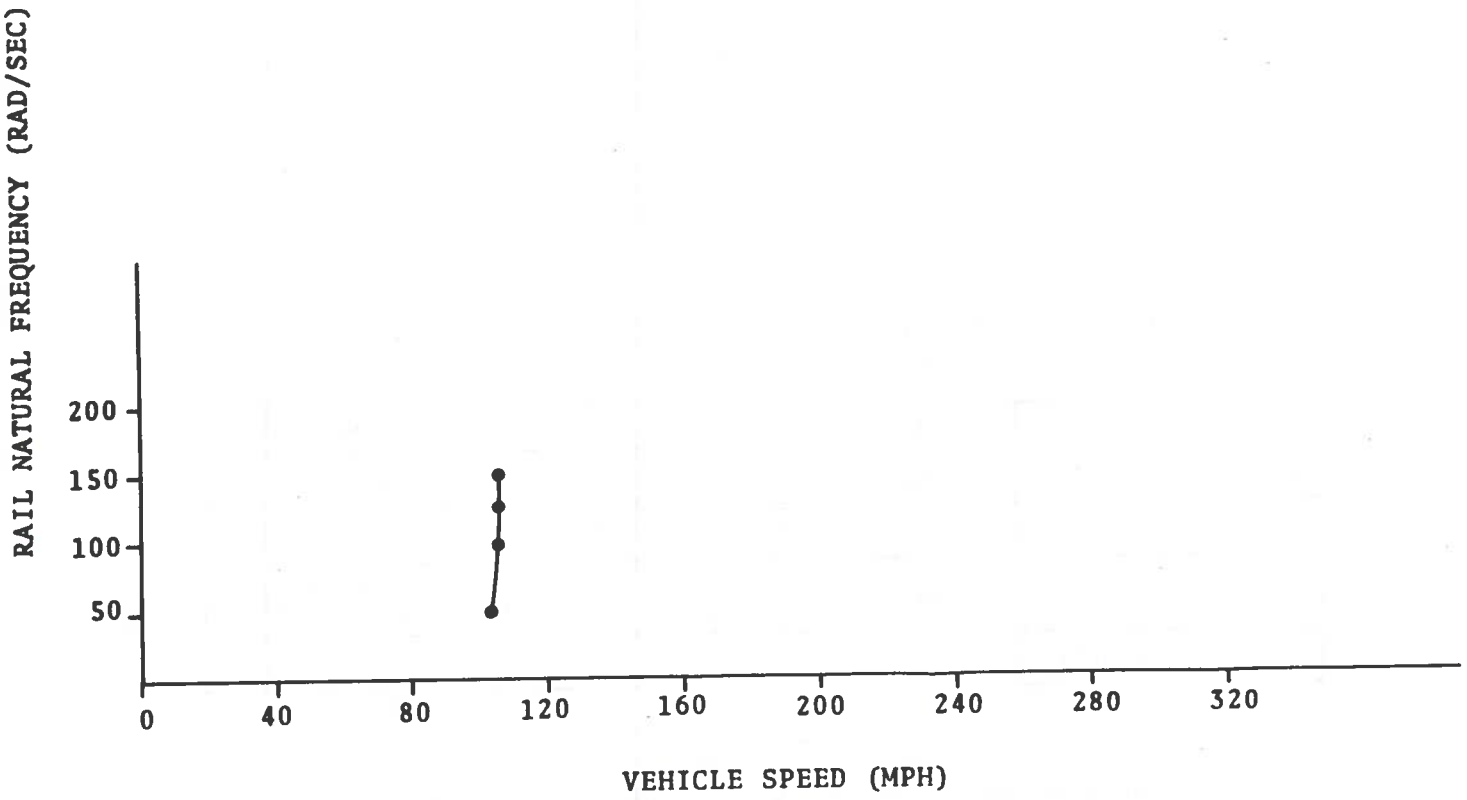

Figure 12 - Collector Resonant Frequency Shift with Rail Natural Frequency

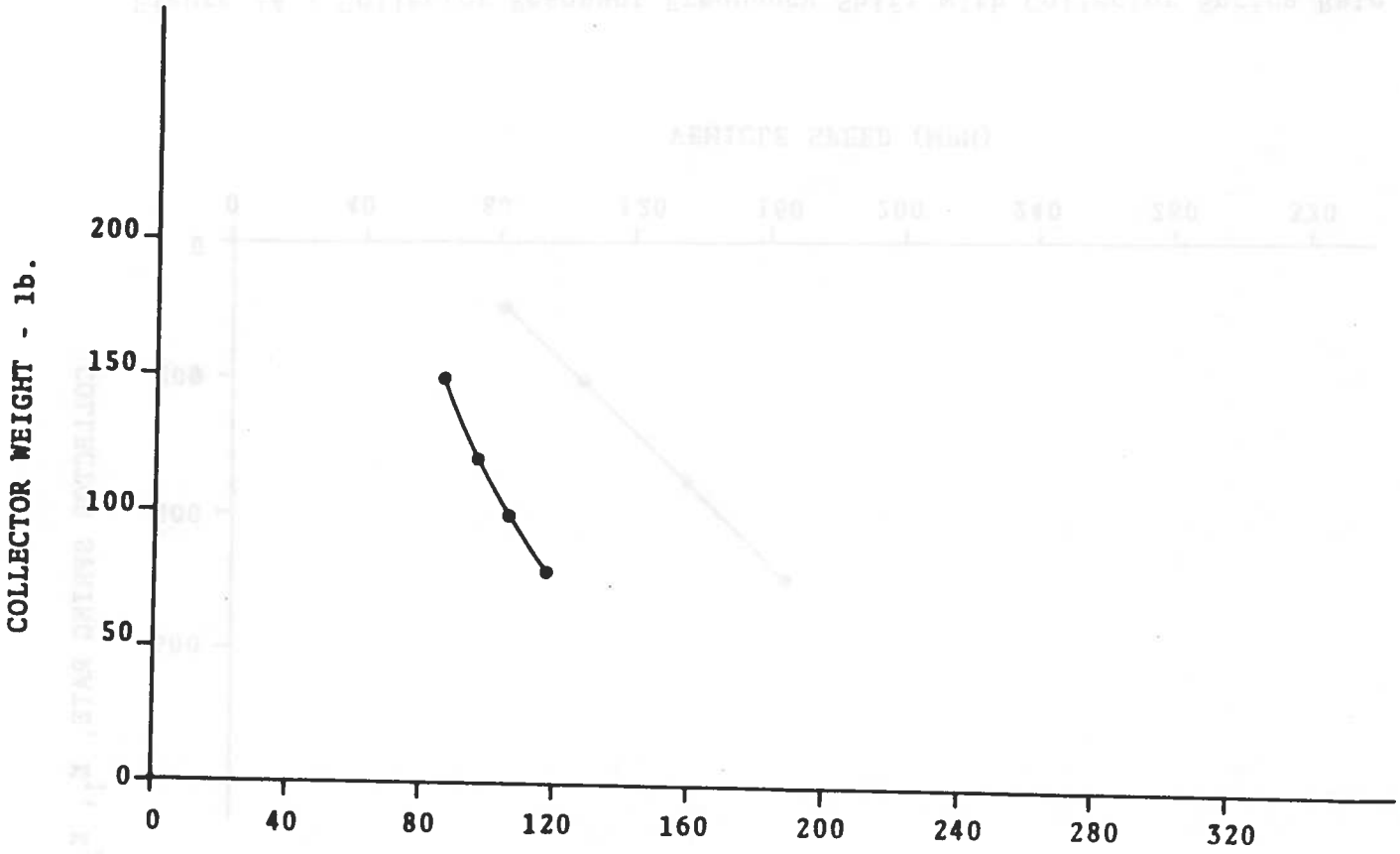

Figure 13 - Collector Resonant Frequency Shift with Collector Weight

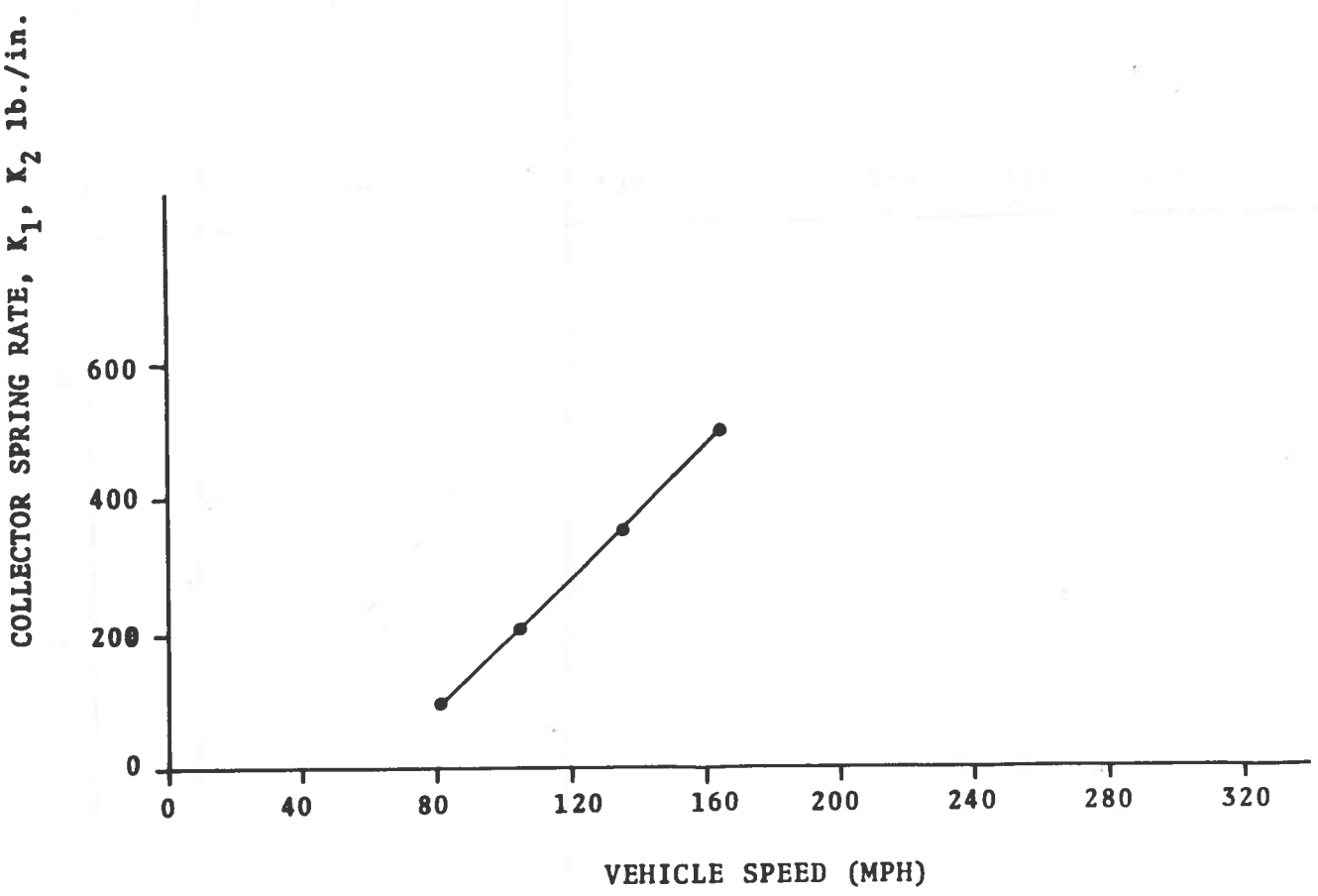

Figure 14 - Collector Resonant Frequency Shift with Collector Spring Rate

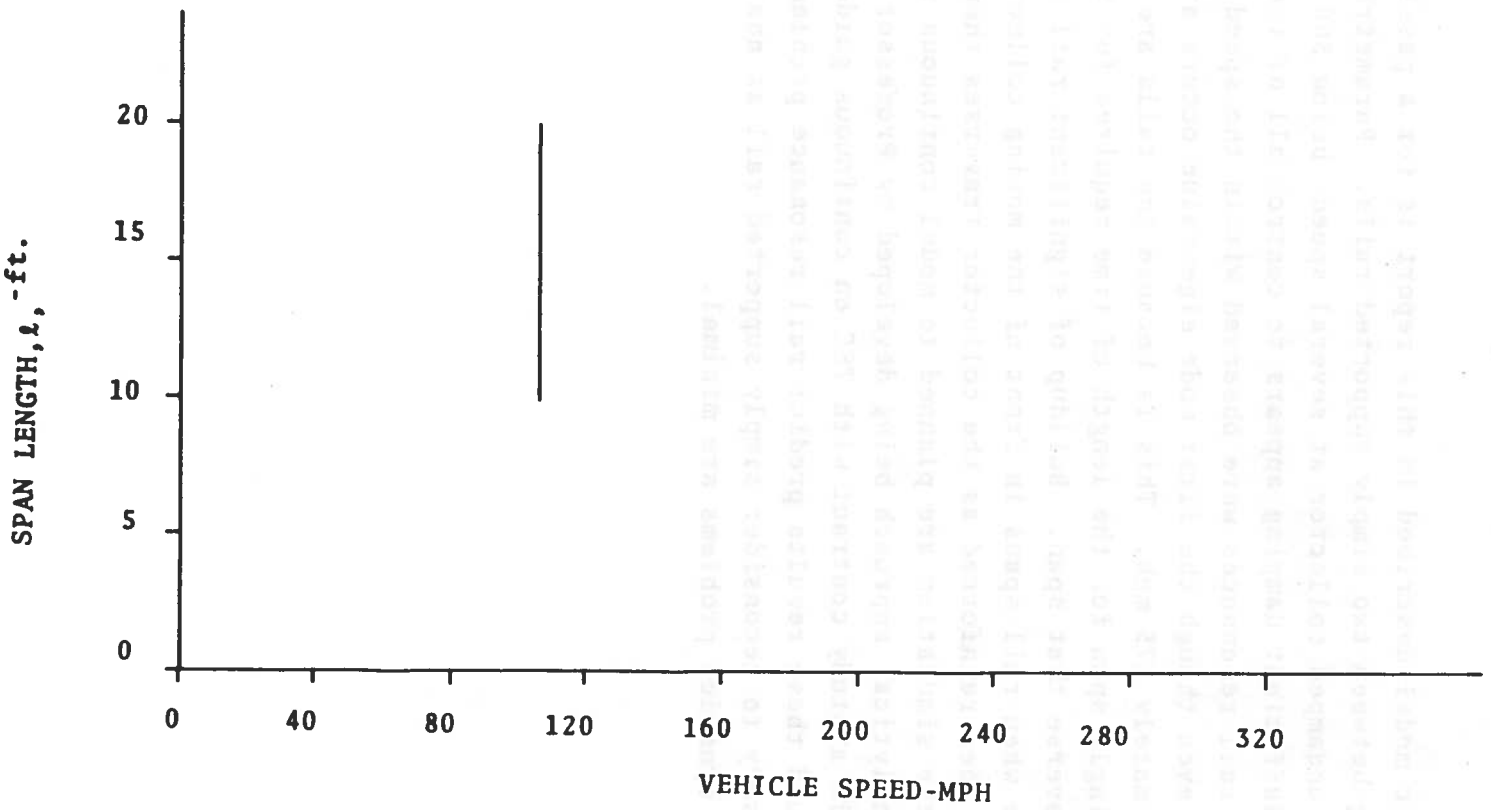

Figure 15 - Collector Resonant Frequency Shift with Span Length

7.0 CONCLUSIONS

The analytic model described in this report is for a passive collector riding between two simply supported rails. Parametric resonance in an undamped collector at several speeds below 300 mph was observed. Sufficient damping appears to control all of these resonances. No rail resonances were observed within the speed range 0-300 mph even though the first mode eigenvalue occurs at a speed of approximately 275 mph. This is because the rails are only forced in any single span for the length of time required for the collector to traverse that span. Buildup of significant rail motion is possible when rail spans in front of the moving collector are excited and then reinforced as the collector traverses them. Alterations to the simulation are planned to model continuous rail, following the analytical approach being developed by Professor Wormley of MIT in a study contract with TSC on continuous guideway modelling. Should these results predict rail resonance problems, it may be necessary to reconsider simply supported rail as analyzed here, since the dynamics problems are minimal.

REFERENCES

1. Chiu, W.S., Smith, R.G., and Wormley, D.N., "Influence of Vehicle and Distributed Guideway Parameters on High Speed Vehicle-Guideway Dynamic Interactions," ASME Paper No. 70-TRAN-13.

2. Blaquière, A., "Nonlinear System Analysis", Academic Press-ing N.Y., 1966.